ACSNANO

www.acsnano.org

ARTICLE

Fabrication of 1D Te/2D ReS_2 Mixed-Dimensional van der Waals *p-n* Heterojunction for High-Performance Phototransistor

Jia-Jia Tao, Jinbao Jiang, Shi-Nuan Zhao, Yong Zhang, Xiao-Xi Li, Xiaosheng Fang, Peng Wang, Weida Hu, Young Hee Lee,* Hong-Liang Lu,* and David-Wei Zhang

Cite This: *ACS Nano* 2021, 15, 3241−3250

Read Online

ACCESS | Metrics & More | Article Recommendations | Supporting Information

ABSTRACT: The superior optical and electronic properties of the two-dimensional (2D) rhenium disulfide (ReS_2) makes it suitable for nanoelectronic and optoelectronic applications. However, the internal defects coupled with with the low mobility and light-absorbing capability of ReS_2 impede its utilization in high-performance photodetectors. Fabrication of mixed-dimensional heterojunctions is an alternative method for designing high-performance hybrid photodetectors. This study proposes a mixed-dimensional van der Waals (vdW) heterojunction photodetector, containing high-performance one-dimensional (1D) *p*-type tellurium (Te) and 2D *n*-type ReS_2, developed by depositing Te nanowires on ReS_2 nanoflake using the dry transfer method. It can improve the injection and separation efficiency of photoexcited electron−hole pairs due to the type II *p*−*n* heterojunction formed at the ReS_2 and Te interface. The proposed heterojunction device is sensitive to visible-light sensitivity (632 nm) with an ultrafast photoresponse (5 ms), high responsivity (180 A/W), and specific detectivity (10^9), which is superior to the pristine Te and ReS_2 photodetectors. As compared to the ReS_2 device, the responsivity and response speed is better by an order of magnitude. These results demonstrate the fabrication and application potential of Te/ReS_2 mixed-dimensional heterojunction for high-performance optoelectronic devices and sensors.

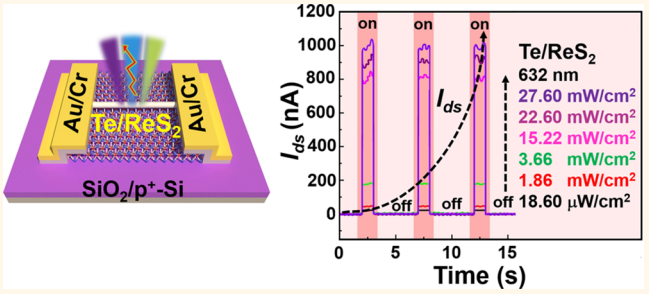

KEYWORDS: *photodetector, visible light, photoresponsivity, ReS_2 nanoflake, Te nanowires, van der Waals heterojunction*

INTRODUCTION

The structures and optoelectronic properties[1−4] of the atomically thin-layered two-dimensional transition metal dichalcogenides (2D TMDs) make it suitable for photodetector application.[5−8] For photoelectronic applications, rhenium disulfide (ReS_2) is the most investigated among the 2D TMDs materials. It has weak interlayer coupling, direct band gap independent of thickness, distorted 1T structure, and low symmetry that enables application in the fabrication of photodetectors and sensors.[9−11] For ReS_2 photodetectors, the highest photoresponsivity (R) and detectivity (D) of 16.14 A/W and 1.30 × 10^{10} Jones, respectively, were achieved in previous studies.[12−15] However, the low mobility of ReS_2 hampers the successful integration of ReS_2-based optoelectronic devices.[16] Many factors determine the mobility of ReS_2 devices, including the scattering of carriers, substrate phonons, interfacial charged impurities, electron−photon coupling, absorbents on the surfaces, and absorption of oxygen and water molecules in the process of device construction.[17,18] In addition, the reduction in the optical absorption of ReS_2 is due to the one-atomic-layer thickness, which makes such monolayer devices inactive in actual application.[19] Thus, improving the performance of the ReS_2 has garnered a lot of attention. Mukherjee et al. presented a multilayer ReS_2/Si *n*−*p* heterojunction with improved photoresponsivity of 33.47 A/W and operation time of 80 μs.[20] Lodha et al. designed WSe_2/ReS_2-based type-II *p-n* heterojunction photodetector, sensitive

Received: November 25, 2020
Accepted: February 2, 2021
Published: February 5, 2021

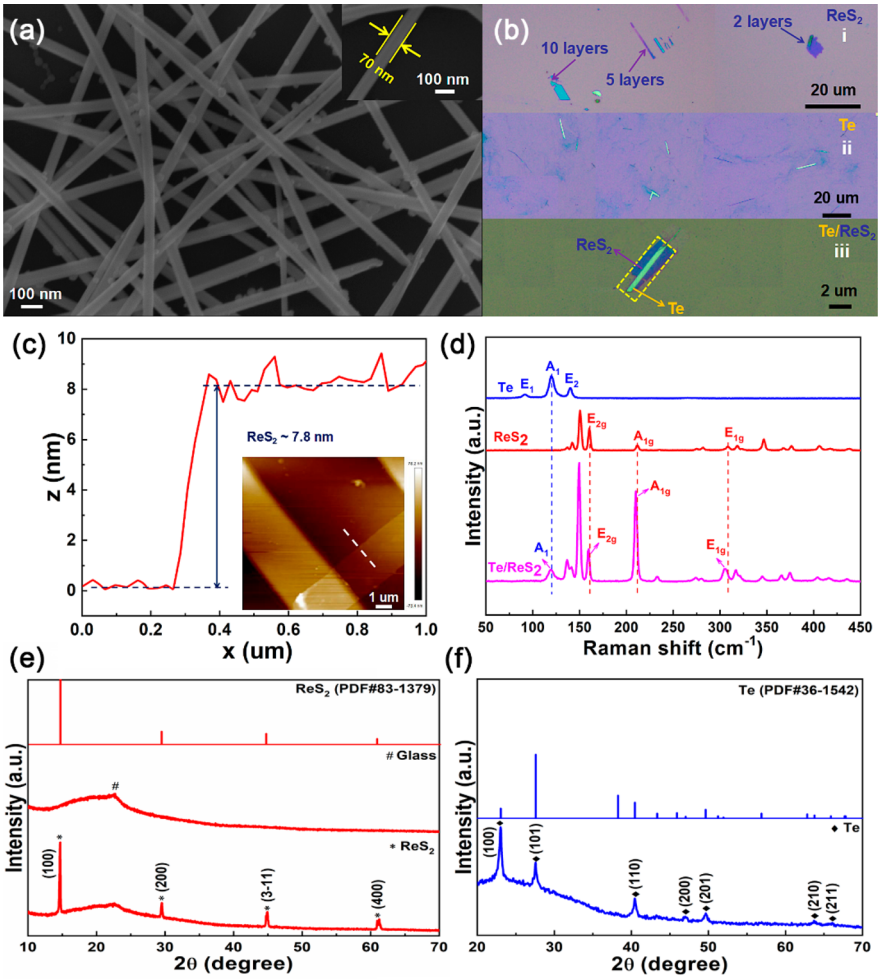

Figure 1. Characterizations of 1D Te/2D ReS_2 mixed-dimensional heterojunction. (a) SEM image of Te NWs. Inset: corresponding enlarged images of the single Te NW. (b) Optical microscope images of (i) 2D ReS_2 NFs with different thicknesses, (ii) single 1D Te NWs of different lengths, and (iii) typical 1D Te/2D ReS_2 mixed-dimensional heterojunction. (c) Typical cross-sectional height profile of the exfoliated ReS_2 NF from the AFM image along the white dashed line shown in the inset. (d) Raman spectra of the pristine Te NWs, ReS_2 NFs, and 1D Te/2D ReS_2 mixed-dimensional heterojunction. XRD patterns of (e) the obtained ReS_2 NFs and (f) Te NWs.

to IR light with the ultrafast response time of 5 μs and high responsivity of 3 A/W.[21] Lee et al. reported a Black Phosphorus (BP)/ReS_2-based type-III $p-n$ heterojunction diode with photoresponsivity of 8 mA/W and external peak quantum efficiency of 0.3%.[22] Lee et al. combined graphene with ReS_2 to fabricate a strong light absorption photodetector with outstanding detectivity of 10^{13} Jones, photoresponsivity of 10^5 A/W, and responsivity of less than 30 ms.[23]

Thus far, only a few studies have focused on the ReS_2 based mixed-dimensional hybrid van der Waals (vdW) heterojunction. Recently, Jariwala et al. proposed mixed-dimensional vdW heterojunctions for overcoming the limitation of electronics of 2D materials.[24] Many research studies have investigated such mixed-dimensional vdW heterojunctions for as an alternate platform for electronics and optoelectronics due to flexibility and high performance. Hu et al. achieved a broadband self-powered photodetector with sensitivity ranging from the UV to visible region by mixed-dimensional 1D Se−2D InSe vdW heterojunction.[25] Ye et al. presented a high-performance dual-channel phototransistor based on a 1D Se/2D ReS_2 heterojunction developed using chemical vapor deposition.[26] Zhang et al. designed 0D−2D mixed vdW heterojunctions of perovskite quantum dots and MoS_2 monolayer for the high-performance phototransistor.[27] Seo et al. investigated the optoelectronic characterization of the $MoSe_2-WSe_2-MoSe_2$ mixed 2D−2D−2D device, which has a high photoresponsivity.[28] Such mixed-dimensional vdW heterojunctions offer exploration possibilities for highly responsive and special optoelectronic applications.

Tellurium (Te) is a p-type semiconductor, a promising material, with high mobility,[29] photoconductivity,[30] piezoelectricity,[31] and thermoelectricity.[32] Though, the single-atomic chain or the few-atomic chains in the Te crystal interacts due to the weak vdW of anisotropic atomic structure.[33] This one-dimensional (1D) vdW crystal structure along with physical properties and stability allows Te application in electronics, optoelectronics, and energy devices. For instance, Zhou et al. demonstrated that Te with high mobility and a deleloped photodetector exhibits high gain and wider operational bandwidth.[34] Javey et al. also fabricated Te on the Au/Al_2O_3 substrate for high-performance short-wave infrared photodetector.[35] Zhai et al. assessed a hydrogen-assisted strategy for preparing Te, and the phototransistor was developed with high-performance gate-dependent photoresponsivity.[36] Besides, the 1D Te metal−semiconductor is also promising for mixed-dimensional vdW heterojunctions, but

https://dx.doi.org/10.1021/acsnano.0c09912
ACS Nano 2021, 15, 3241−3250

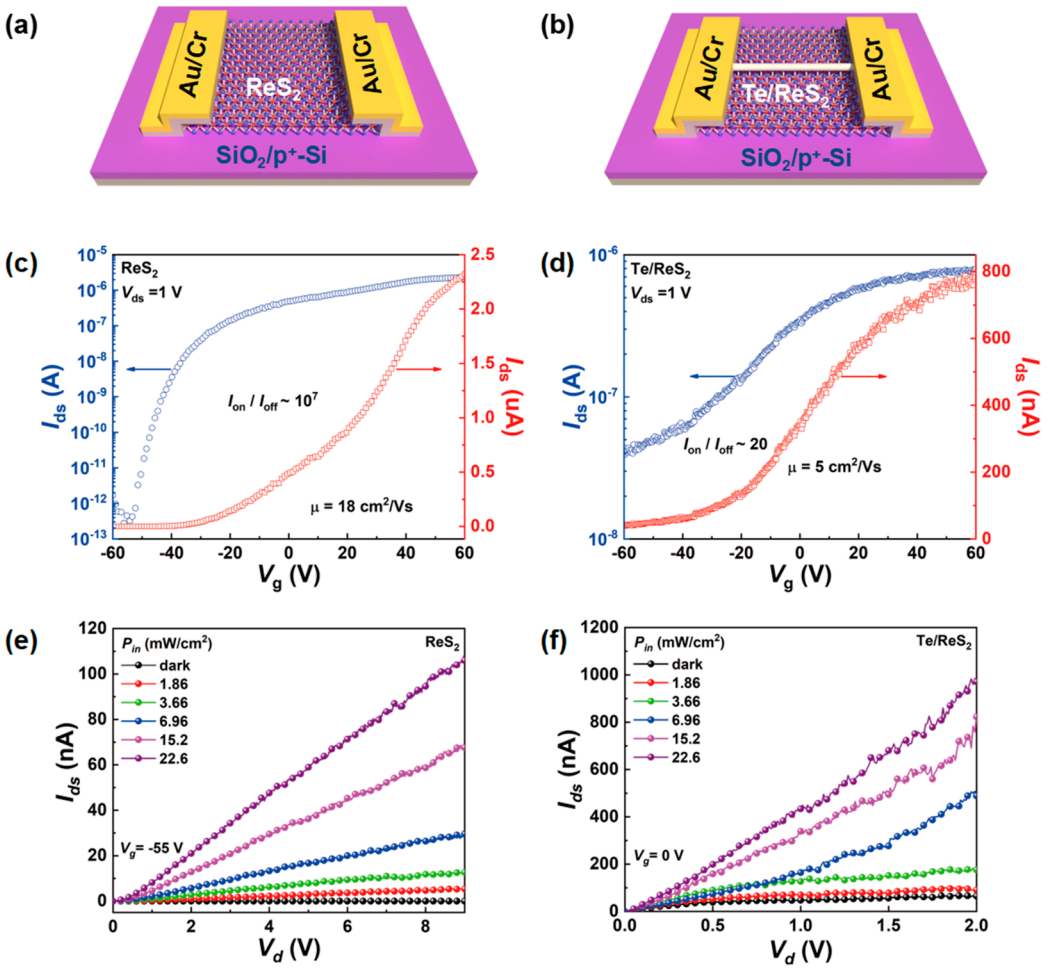

Figure 2. Schematic structure, transfer, and output characteristics of ReS_2 and Te/ReS_2 FETs under dark and light conditions. Schematic structure of (a) ReS_2 and (b) Te/ReS_2 phototransistors. (c,d) I_{ds}−V_g curves of FETs at V_d = 1 V in the dark. (e,f) I_{ds}−V_d curves with variable light power intensity (632 nm) at V_g = −55 V for ReS_2 and 0 V for Te/ReS_2 FETs. Figure S3a−c depict the I_{ds}−V_d curves of FETs at V_g of 0 V to reveal the contact behaviors.

there is a lack of research on the photoelectric detection technology combining 2D materials with 1D Te nanowires (NWs). Further, the unclear interaction mechanism of 2D materials and 1D Te in the vdW heterojunctions hamper prospects in optoelectronic applications.

This study demonstrates a mixed-dimensional vdW heterojunction of 1D *p*-type Te NW and 2D *n*-type ReS_2 nanoflake (NF) for photoelectric detection applications. The Te NWs were first prepared by a facile hydrothermal method and then transferred to the ReS_2 NFs layer using the dry transfer method. Subsequently, this study evaluated, in the context to the photodetector performance, the electrical properties of the proposed dual-channel field-effect transistors (FETs). Compared to 2D ReS_2 NF, the 1D Te/2D ReS_2 heterojunction shows a significant improvement in light absorption, an increase in the electron−hole pair concentration, and the improved injection and separation efficiency of electron−hole pairs at the interface. This significant improvement is due to the light trapping effect, type II band alignment, and built-in electric field in the constructed Te/ReS_2 heterojunction. The photoresponsivity and photoresponse rate of the Te/ReS_2 heterojunction photodetector are superior to the bare Te or ReS_2 devices. Therefore, the 1D Te/2D ReS_2 heterojunction is a valuable addition to the array of mixed-dimensional *p*−*n* heterojunction, which has widened the scope of the implementation in optoelectronics and sensor applications.

RESULTS AND DISCUSSION

Material Characterization. Figure 1a depicts the SEM image of the synthesized Te sample. The Te NWs with a length of more than 10 μm appear uniformly on the silicon substrate. Besides, as depicted in the set of Figure 1a, the diameter of Te NW is about 70 nm. The calculated aspect ratio of Te is 200, which indicates the anisotropy of Te NWs, and the smooth surface of Te NWs indicates high purity and quality. Figure 1b demonstrates the optical images of ReS_2 NFs, the as-grown Te NWs, and Te/ReS_2 heterojunction. Part (i) depicts the different thicknesses of ReS_2 NFs distinguishable by the optical contrast. Part (ii) depicts the easy separation of single Te NW and multiple NWs, which are the conditions for successful transfer and device fabrication. A single nanowire with a thicker diameter is formed by clustering multiple single nanowires. Part (iii) depicts the single Te NW with a thicker diameter that is tightly attached to ReS_2 NF, forming a Te/ReS_2 heterojunction. Figure 1c and its insets show the measured corresponding thickness and AFM image of ReS_2, respectively. The thickness of ReS_2 NFs for the

https://dx.doi.org/10.1021/acsnano.0c09912
ACS Nano 2021, 15, 3241−3250

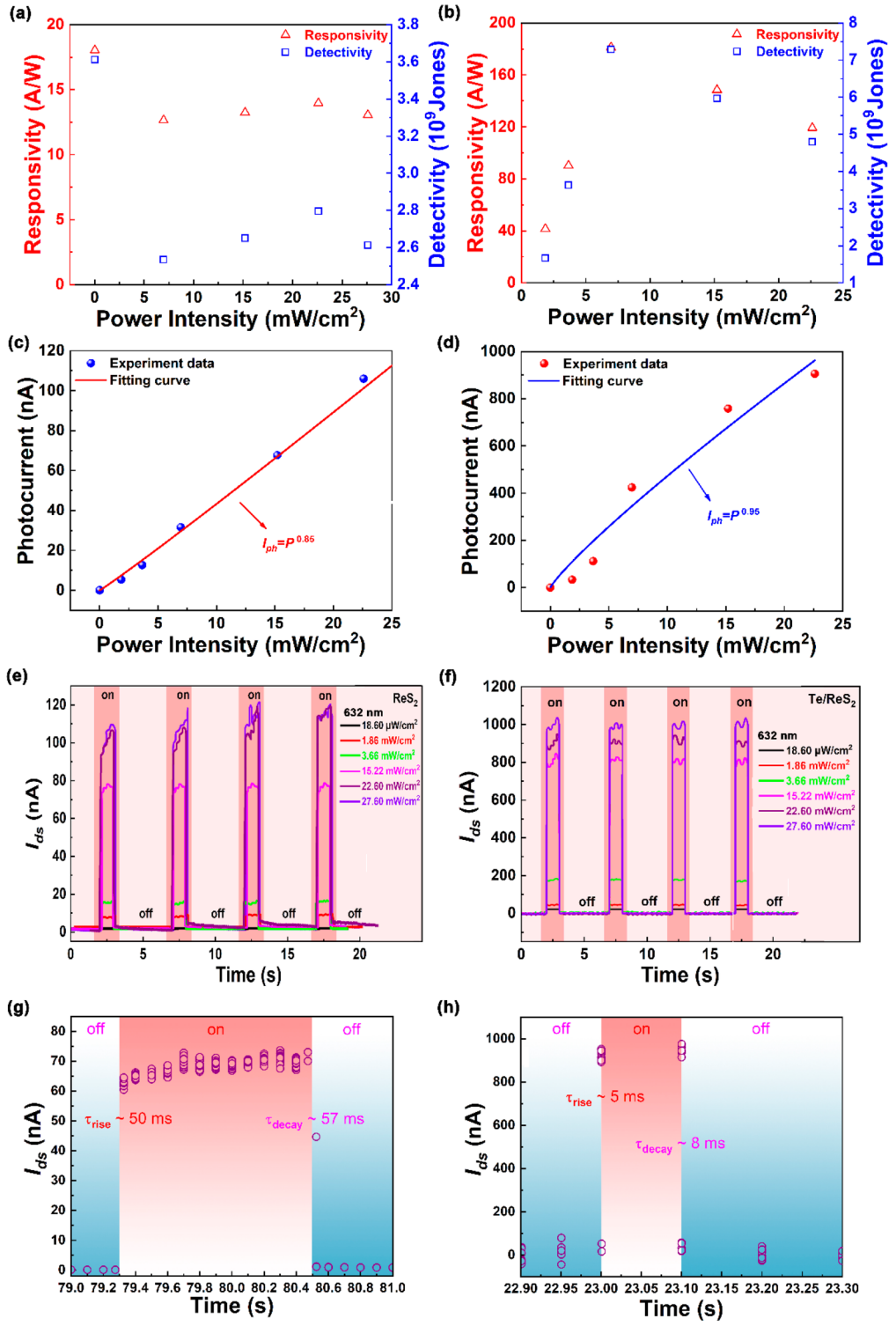

Figure 3. Optoelectronic performance characterization of the ReS_2 and Te/ReS_2 photodetectors. (a, b) Responsivity and detectivity and (c, d) experimental and fitted photocurrent of devices as a function of the illumination intensity. (e, f) Time-dependent photocurrent response under switched-on/off light irradiation with different power intensities at V_d of 9 and 2 V and V_g of −55 and 0 V for ReS_2 and Te/ReS_2, respectively. (g, h) Temporal illumination response of the single on/off cycle highlights τ_{rise} and τ_{decay} time under an illumination intensity of 15.22 mW/cm^2.

fabrication of devices is estimated to be 7.80 nm, which is appropriate as per the previously reported best optoelectronic performance.[37] Besides, no air bubbles in the overlapping heterojunction region indicate a strongly coupled Te and ReS_2 interface.

Figure 1d depicts the Raman spectra of Te, ReS_2, and Te/ReS_2 heterojunction. Specifically, for pristine Te (blue color spectrum), the three peaks at 92, 120, and 140 cm^{-1} are the respective characteristic peaks of the E_1, A_1, and E_2 modes, as per the previous results.[38] For pristine ReS_2 (red color

https://dx.doi.org/10.1021/acsnano.0c09912
ACS Nano 2021, 15, 3241−3250

spectrum), the three Raman peaks at 160, 308, and 211 cm^{-1} correspond to the E_g modes (in-plane vibration) and A_{1g} mode (out of plane vibration), respectively. These peak positions are as per the reported Raman results of ReS_2.[39] All the peaks of Te and ReS_2 presented in the constructed Te/ReS_2 interface indicate the formation of a Te/ReS_2 heterojunction. However, compared to the Raman peaks in pristine ReS_2, minor blue shifts are observed in the Raman peaks in Te/ReS_2 due to the vdW interaction between top Te NW and bottom ReS_2 NF.[40] No apparent peak-shifts in the Raman peak positions of Te unveil the high-quality monolayer Te after fabrication of the vdW heterojunction. Diffraction peaks in Figure 1e validate the presence of triclinic phase ReS_2 (PDF no. 89-1379).[41] Figure 1f shows the XRD patterns of Te NWs, with the diffraction peaks as per the hexagonal Te (PDF no. 36-1542).[42] Besides, a lack of other impurity peaks establishes the superior crystallinity and purity of the as-grown Te NWs and ReS_2 NFs.

Figure S1 schematically illustrates the fabrication process of the Te/ReS_2 heterojunction photodetector. In addition, the experimental methods of the Supporting Information detail the process. First, the use of the two-step dry transfer provides the integrated Te/ReS_2 heterojunction. This method also establishes an intimate bonding between Te NW and ReS_2 NF. The vertical device structures obtained have four levels, ReS_2-on-SiO_2/p^+-Si substrate, Te NF, and top Au/Cr electrodes. Subsequently, for the systematic comparison, the individual Te and ReS_2 PDs are also fabricated. Figure S2 depicts the SEM and optical microscope images of all devices.

Figure S3 depicts the $I_{ds}-V_d$ curves at V_g of 0 V investigating the contact behaviors of FETs. The contacts at source/drain demonstrate Schottky behaviors of the Te NWs device at room temperature, while the ReS_2- and Te/ReS_2-based FETs demonstrate typical Ohmic behaviors. Parts a and b of Figure 2 depict the schematic structures of the devices. Parts c and d of Figure 2 show the transfer characteristics ($I_{ds}-V_g$) on linear and semilogarithmic scales of ReS_2 and Te/ReS_2 FETs at the V_{ds} = 1 V in the dark. As depicted in Figure 2c, the ReS_2-based FET showed excellent *n*-type behaviors with a high on/off ratio ($\sim 10^7$) and a low off-state current (10^{-13} A). The observed threshold voltage (V_{th}) of nearly −30 V suggests large electron concentration or natural *n*-doping for ReS_2 device, which results from S vacancies or impurities of ReS_2 NFs.[43] Conversely, as depicted in Figure 2d, the Te/ReS_2 FETs show a poor on/off ratio (~20) and high off-state current (10^{-8} A). As compared to the ReS_2 FETs, V_{th} for Te/ReS_2 FETs shows a red shift from −30 to −20 V. At V_g = 60 V and V_{ds} = 1 V, compared to ReS_2 FETs, the on-state current of Te/ReS_2 FETs presents an order of magnitude decrease, which could significantly reduce the testing noise and enhance the detectivity of photodetectors. Such electrical behavior changes indicate that the hole carriers of *p*-type of Te flakes dominate the transport properties of Te/ReS_2 FETs, which attributes to the distinct *p*-doping effect of vertical stacked 1D Te NWs on the underlying 2D ReS_2 NFs. In addition, the transfer characteristic of Te was demonstrated in Figure S4 and a conspicuous *p*-type behavior was observed, which shows poor performance with low on/off ratio of about 10. The following relation provided the field-effect carrier mobility (μ):

$$\mu = \frac{L}{W}\left(\frac{dI_{ds}}{dV_g}\right)\frac{1}{C_g V_{ds}} \quad (1)$$

Among them, *L*, *W*, (dI_{ds}/dV_g), and C_g are the channel length, channel width, slope of the transfer characteristics, and gate capacitance of the Si/SiO_2 substrate, respectively. Mobility for ReS_2 and Te/ReS_2 FETs was 18 and 5 $cm^2/(V\ s)$, respectively. The mobility of Te/ReS_2 FETs was much lower than that of ReS_2 FETs, similar to the previously reported values for other ReS_2-based FETs.[26]

The laser diodes, as the light source, operating at a wavelength of 632 nm with different optical power densities (P_{in}), investigated the optoelectronic properties of Te, ReS_2, and Te/ReS_2 FETs. Figure S5 presents the V_g-I_{ds} characteristics of ReS_2 and Te/ReS_2 devices at different light intensities. It shows that maximum change values in I_{ds} before and after illumination occur at a V_g of −55 and 0 V for ReS_2 and Te/ReS_2 FETs, respectively. Figure S6 depicts optoelectronic properties of the Te NWs device, exhibiting a nonobvious response under 22.6 $mW{\cdot}cm^{-2}$ illumination. Subsequently, parts e and f of Figure 2 show the $I_{ds}-V_d$ curves of ReS_2 and Te/ReS_2 devices under different optical power densities (P_{in}) of illumination and dark, respectively. It revealed that the dark current (I_{dark}) did not change much with increasing V_{ds} under no light illumination for all devices. At V_{ds} = 9 V, the I_{dark} was only 0.26 pA for ReS_2 FETs and 65.02 nA for Te/ReS_2 at V_{ds} = 0 V. Thus, all devices depicted a distinct photoresponse, where I_{ds} gradually increases with an increase in P_{in} from 1.86 to 22.6 mW/cm^2. As compared to the Te device, Te/ReS_2 device had higher I_{ds} even at low P_{in} (1.86 mW/cm^2), indicating a highly sensitive photodetection for the visible range (632 nm).

For photodetectors, responsivity (*R*) and detectivity (*D*) are critical parameters represented by the following equations[44]

$$R = \frac{I_{photo} - I_{dark}}{P_{in}A} \quad (2)$$

where I_{photo} is the measured photocurrent, I_{dark} is the dark current, and P_{in} and *A* are the light illumination intensity and active area.

$$D = \frac{R}{(2qI_{dark}/A)^{1/2}} \quad (3)$$

Among them, *q* represents the elementary charge. Parts a and b of Figure 3 show the calculated *R* and *D* under various incident power densities for ReS_2 and Te/ReS_2 heterojunction photodetectors. The maximum *R* and *D* of the ReS_2 device are 20 A/W and 3.6×10^9 Jones, respectively, at V_d = 1 V, and V_g = −55 V with the power density of 18.60 $\mu W/cm^2$, which is higher the other ReS_2 photodetectors.[7] Further, at the V_d = 1 V and power density of 18.60 $\mu W/cm^2$, *R* of the Te/ReS_2 heterojunction photodetector was 180 A/W, which was one order higher than that of ReS_2 photodetector. Besides, the *D* of the Te/ReS_2 photodetector is 7.2×10^9 Jones, which promoted by two times compared to ReS_2 photodetector. The *D* is influenced by the defects of ReS_2 from S vacancies in Te/ReS_2 heterojunction, which leads the high dark current. Nonetheless, the 10^9 Jones of *D* is comparable with other reported composite structures.[45,46] For the device defects verification, the incident light intensity-dependent photocurrent curves are as per the following power law[47]

$$I \propto P^{\theta} \quad (4)$$

where *I* is the photocurrent, *P* is the light intensity, and θ is the power exponent. As depicted in Figure 3c,d, the power exponent (θ) is 0.85 and 0.95 for ReS_2 and Te/ReS_2

https://dx.doi.org/10.1021/acsnano.0c09912
ACS Nano 2021, 15, 3241−3250

Table 1. Performance Parameters Comparison of Photodetectors based on 1D Te NWs and 2D ReS_2 NFs with Other Mixed-Dimensional Heterojunction Photodetectors Reported in the Literature

photodetector	wavelength (nm)	responsivity (A/W)	detectivity (Jones)	rise time (s)	decay time (s)	refs
2D ReS_2 nanoflakes	220	13		6	21	11
1D ReS_2 nanowires	500	5.08×10^5	6.1×10^{15}	1.8	3.9	14
2D Te nanosheets	261	6.5×10^4	3.73×10^8	2	5	52
1D/2D Se/InSe	460	32	1.7×10^{11}	0.030	0.037	25
1D/2D t-Se/ReS_2	400	98	6×10^{10}	0.05	0.05	26
1D/1D Te/TiO_2	350	0.084	3.7×10^9	0.772	1.492	53
1D/2D Se/ReS_2	370	36	8×10^{12}	0.01	0.01	45
1D/2D Sb_2Se_3/WS_2	520	1.51	1.16×10^{10}	0.008	0.008	50
2D/2D CdS/MoS_2	610	3.91		0.01	0.01	54
1D/1D ZnO/Co_3O_4	solar light	21.80	4.12×10^{12}	6	6	55
2D ReS_2 nanoflakes	632	20	3.6×10^{11}	0.05	0.057	this work
1D/2D Te/ReS_2	632	180	5×10^9	0.005	0.008	this work

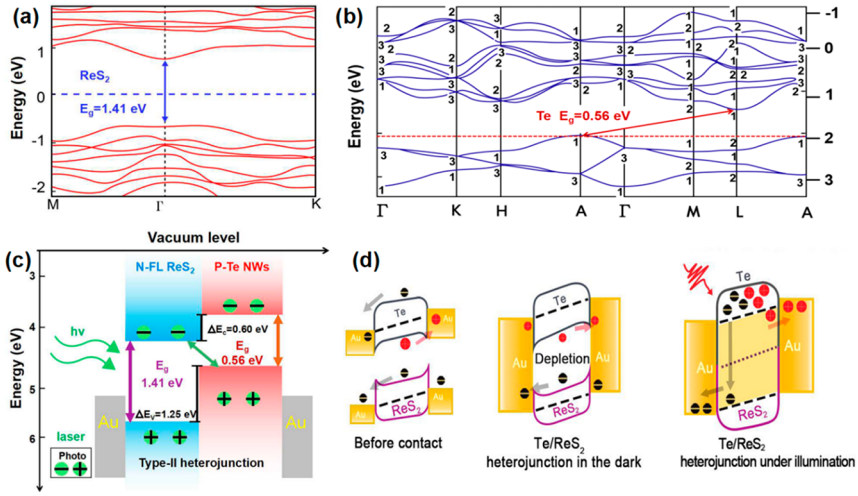

Figure 4. Electronic band structures of (a) ReS_2, and (b) Te. (c) Band alignment of the Te/ReS_2 heterojunction. (d) Energy band diagram and carrier transport of the Te and ReS_2 for before contact, after contact, and under light irradiation. The Fermi energy is set as zero energy.

heterojunction, respectively. For the ReS_2 photodetector, the sublinear response curve with light intensity indicates that the photogenerated carrier recombination due to intrinsic defects or the charge impurities at the surface of the ReS_2.[48] Moreover, the calculated θ of Te/ReS_2 is higher than ReS_2, which suggests the fewer recombination centers exist in the heterojunction. These results are dependent on the charge impurities around the ReS_2 with reduced after Te covering compared to intrinsic ReS_2. Besides, the part of the surface of ReS_2, previously occupied by O_2/H_2O, was drastically covered by the Te/ReS_2 interfaces due to surface recombination sites.[49] A similar sublinear dependence in Se/InSe and Sb_2Se_3/WS_2 vertical bilayer heterostructures have been previously reported.[25,50]

The response speed includes the on/off current ratio, and the rise and decay time is another vital parameter for photodetector. This study further assessed the time dependence of photocurrent with the laser turning on or off for demonstrating the device response speed. As depicted in Figure 3e,f, upon illumination, the device current generated increases sharply, then stabilizes in a higher current, and finally vanishes in the dark, which is steady and reproducible over the repeated cycles, exhibiting excellent stability and reliability of all devices. Moreover, the photoswitching on/off ratio of Te/ReS_2 (1000) is significantly higher than that the ReS_2 device (200), which is similar to the V_d–I_{ds} results demonstrated in Figure 2e,f. The time taken by the pulse amplitude to rise from 10% to 90% of the maximum value and vice versa is the rise and decay time of devices. Further, the on/off current ratio and the rise and decay times of device were characterized and depicted in Figure 3g,h. For ReS_2, the rise and decay times were nearly 50 and 57 ms, respectively. The rise and decay times for the Te/ReS_2 device under illumination was equal or less than 5 and 8 ms, which was beyond the measurement capability of the equipment used. Compared to the bare ReS_2 photodetector, seven to ten times faster rising and decaying time was exhibited by the Te/ReS_2 heterojunction photodetector. This excellent performance can be due to the Te NWs acting as the absorption layer and the built-in electric field inducement, aiding in efficient photocarrier extraction from the Te/ReS_2 heterojunction.[51] Optoelectronic performance parameters comparison of Te/ReS_2 photodetector with other mixed-dimensional visible heterojunction photodetectors reported in the literature demonstrated similarity and improvement (Table 1). It suggests a promising application of the proposed Te/ReS_2 for highly efficient visible photodetection.

The electronic band structures of ReS_2 and Te calculated by density functional theory are shown in Figure 4a,b. The calculation details are provided in Supporting Information. From the calculated results, the ReS_2 has a direct band gap of 1.41 eV, corresponding to the other reported result.[56] For Te, the results display the band gap of 0.56 eV, which is in accord

https://dx.doi.org/10.1021/acsnano.0c09912
ACS Nano 2021, 15, 3241−3250

with the reported value.[57] As shown in Figure 4c, both the conduction band maximum (CBM) and valence band minimum (VBM) of Te are higher than that of ReS_2. Thus, the Te/ReS_2 heterojunction have a type II band alignment. Figure 4d demonstrates the photocarriers transmission of Te/ReS_2 heterojunction under dark and light. Under dark conditions, Au, ReS_2, and Te have different Fermi energies formation before contact with each other. The contact of ReS_2 and Te with Au forms the low Schottky barriers at the interfaces. The charge transfer and electron−hole recombination occurred at the Te/ReS_2 interface during the Te/ReS_2 heterojunction formation. This behavior of charge transmission lowers/raises the Fermi level of ReS_2 (Te), causing the formation of depletion regions and introducing a built-in field toward ReS_2. The depletion region formation accompanied by the Schottky barrier reduction at the Au/ReS_2 (Au/Te) interfaces significantly suppresses the dark current in the heterojunction bilayers.[58] The light illumination causes the generation of electron−hole pairs in the Te NWs; thereby the electrons are transferred to ReS_2 NFs, and photoexcited holes in ReS_2 NFs transfer to Te NWs. The charge separation is beneficial in reducing electrons and holes recombination, which enhancing the photogenerated current. This phenomenon raises the Fermi level in ReS_2 NFs while lowers that of Te NWs. The accumulated electrons (holes) in ReS_2 NFs (Te NWs) could transport through the two channels driven applied electric field of V_{ds} and be captured immediately by the electrodes, resulting in a high photocurrent.

Meanwhile, the reduced Schottky barriers at the contact interfaces (Au/ReS_2 and Au/Te) account by modulation of Fermi level also facilitate the carrier injection and enhances the channel current.[59] The ReS_2 can bond with gas molecules for the high chemical activity of Re atom. As a result, the trap states in the band gap generate that will a poor photoresponse speed.[60] The introduction of Te NWs enhances the absorption of light and causes surface defects of ReS_2, which significantly increases the photocurrent. Furthermore, the Re−Te bond at the interface provides a direct path for carrier separation and transfer, which accelerated the response speed.[61]

CONCLUSIONS

In summary, this study proposes a fabricated 1D Te/2D ReS_2 mixed-dimensional van der Waals p−n heterojunction using hydrothermal, mechanical exfoliation, and dry transfer methods. This study had explored the electronic and optoelectronic properties of Te NWs, ReS_2 NFs, and their heterojunction devices. Compared to the pristine Te and ReS_2 photodetectors, the Te/ReS_2 heterojunction photodetector has superior performance with excellent responsivity (180 A/W), high specific detectivity (10^9), and short photoresponse time (5 ms). The responsivity and response time are higher by 1 order of magnitude than the ReS_2-alone device. These improvements are due to the benefits from the type-II band alignments, enhanced light absorption, and passivate surface effect of heterojunction, which also rapidly separates the photogenerated electron−hole pairs. The performance improvements reported in this study can provide a fabrication method of mixed-dimensional van der Waals heterojunction for optoelectronic applications.

EXPERIMENTAL SECTION

Growth of 1D Te NWs. To construct 1D Te/2D ReS_2 mixed-dimensional heterojunction, first the Te NWs were synthesized by the hydrothermal method as previously reported.[53] This process provides Te NWs of controlled diameters and lengths. All the chemicals in the experiment were weighed using a METTLER TOLEDO ME 204 balance. Furthermore, Te NWs synthesized by the hydrothermal method have demonstrated excellent optical and electrical properties, which show potential for photodetector application.[62,35]

Fabrication of the Heterojunction Photodetectors. First is the alcohol dispersion of the as-prepared Te NWs, and next is the coating on a SiO_2 (280 nm)/p^+-Si wafer by a spin-coating method for transfer process. Simultaneous is the mechanical exfoliation of ReS_2 NFs from a ReS_2 bulk (Six Carbon Technology Supplies) onto the SiO_2 (280 nm)/p^+-Si substrate with a scotch-tape method. The ReS_2 NFs of 7−8 nm thickness on the proper lateral size of the substrate was selected for the heterojunction fabrication. Later, Te NWs transferred onto the ReS_2/Si substrate by a dry transfer method with the help of accurate transfer platform (Metatest, E1-T), froms the 1D Te/2D ReS_2 mixed-dimensional heterojunction. For the fabrication of Te, ReS_2, and Te/ReS_2 devices, source-drain electrodes were defined by the electron beam lithography and followed by the deposition of Cr/Au with 10/70 nm deposited by physical vapor deposition equipment, followed by a lift-off process in acetone.

Characterizations and Measurements of Photodetectors. An X-ray diffractometer (Bruker, D8) was used to determine the crystalline structure of samples. Raman spectroscopy (Lab RAM HR800, Horiba Jobin Yvon) with an excitation wavelength of 532 nm analyzed the optical properties. The thickness and surface morphology of samples were measured by AFM (Dimension Icon, Bruker) in tapping mode and SEM (Sigma HD, Zeiss), respectively. The electrical performance measurement was by a semiconductor parameter analyzer (Keysight, B1500) in a robe station (Lake Shore). For photodetector performance measurements, a light source of 632 nm laser diode (Thorlabs, LD632P70MLD) evaluated the photoresponse. The laser first passes through the collimator to obtain a parallel beam, which then shines onto the device channel. The laser switch controlling is by the laser controller (Thorlabs, LDC4001), which can achieve photoresponse speed measurement. The signal was amplified through a lock-in amplifier (Stanford, SR570) and then detected by a digital oscilloscope.

ASSOCIATED CONTENT

Supporting Information

The Supporting Information is available free of charge at https://pubs.acs.org/doi/10.1021/acsnano.0c09912.

Experimental methods, schematic for the fabrication process of Te, ReS_2, and Te/ReS_2 FET based phototransistors, SEM and optical microscope images of ReS_2 and Te/ReS_2 devices, I_{ds}−V_d curves at V_g of 0 V of Te, ReS_2, and Te/ReS_2 devices, transfer curve of Te FET measured under dark at V_{ds} = 1 V, V_g−I_{ds} characteristics of ReS_2 and Te/ReS_2 devices at different light intensity with the wavelength of 632 nm, and I_d−V_d of pure Te device under dark conditions and at maximum light intensity of 22.6 mW/cm^2 with the wavelength of 632 nm (PDF)

AUTHOR INFORMATION

Corresponding Authors

Young Hee Lee − *Center for Integrated Nanostructure Physics (CINAP), Institute for Basic Science (IBS), Department of Energy Science, Department of Physics, Sungkyunkwan University, Suwon 16419, Republic of Korea;* orcid.org/0000-0001-7403-8157; Email: leeyoung@skku.edu

Hong-Liang Lu − *State Key Laboratory of ASIC and System, Shanghai Institute of Intelligent Electronics & Systems, School of Microelectronics, Fudan University, Shanghai 200433,*

https://dx.doi.org/10.1021/acsnano.0c09912
ACS Nano 2021, 15, 3241−3250

China; orcid.org/0000-0003-2398-720X;
Email: honglianglu@fudan.edu.cn

Authors

Jia-Jia Tao − *State Key Laboratory of ASIC and System, Shanghai Institute of Intelligent Electronics & Systems, School of Microelectronics, Fudan University, Shanghai 200433, China*

Jinbao Jiang − *Center for Integrated Nanostructure Physics (CINAP), Institute for Basic Science (IBS), Department of Energy Science, Department of Physics, Sungkyunkwan University, Suwon 16419, Republic of Korea*

Shi-Nuan Zhao − *Collaborative Innovation Center of Advanced Microstructures, State Key Laboratory of Applied Surface Physics, Department of Physics, Fudan University, Shanghai 200433, China*

Yong Zhang − *Department of Materials Science, Fudan University, Shanghai 200433, China*

Xiao-Xi Li − *State Key Laboratory of ASIC and System, Shanghai Institute of Intelligent Electronics & Systems, School of Microelectronics, Fudan University, Shanghai 200433, China*

Xiaosheng Fang − *Department of Materials Science, Fudan University, Shanghai 200433, China;* orcid.org/0000-0003-3387-4532

Peng Wang − *State Key Laboratory of Infrared Physics, Shanghai Institute of Technical Physics Chinese Academy of Sciences, Shanghai 200083, China*

Weida Hu − *State Key Laboratory of Infrared Physics, Shanghai Institute of Technical Physics Chinese Academy of Sciences, Shanghai 200083, China;* orcid.org/0000-0001-5278-8969

David-Wei Zhang − *State Key Laboratory of ASIC and System, Shanghai Institute of Intelligent Electronics & Systems, School of Microelectronics, Fudan University, Shanghai 200433, China*

Complete contact information is available at: https://pubs.acs.org/10.1021/acsnano.0c09912

Author Contributions

J.T., J.J., and Y.Z. designed the research. S.Z. and X.L. performed the XRD and Raman measurements. X.F. and P.W. contributed to device fabrication. W.H., Y.L., L.L., and D.Z. assisted with data analysis. J.T. wrote the paper, and all authors commented on the manuscript.

Notes

The authors declare no competing financial interest.

ACKNOWLEDGMENTS

This work is supported by the National Natural Science Foundation of China (Nos. 61874034, 51861135105, and U1632121) and the Natural Science Foundation of Shanghai (No. 18ZR1405000). This work is also supported by the Fudan University Exchange Program Scholarship for Doctoral Students (No. 2019026). The authors thank Prof. Yi-Fang Chen, Fudan University, for the scanning electron microscopy tests.

REFERENCES

(1) Dai, M. J.; Chen, H. Y.; Feng, R.; Feng, W.; Hu, Y. X.; Yang, H. H.; Liu, G. B.; Chen, X. S.; Zhang, J.; Xu, C. Y.; Hu, P. A. A Dual-Band Multilayer InSe Self-Powered Photodetector with High Performance Induced by Surface Plasmon Resonance and Asymmetric Schottky Junction. *ACS Nano* **2018**, *12*, 8739−8747.

(2) Dai, M. J.; Zheng, W.; Zhang, X.; Wang, S. M.; Lin, J. H.; Li, K.; Hu, Y. X.; Sun, E. W.; Zhang, J.; Qiu, Y. F.; Fu, Y. Q.; Cao, W. W.; Hu, P. A. Enhanced Piezoelectric Effect Derived from Grain Boundary in MoS_2 Monolayers. *Nano Lett.* **2020**, *20*, 201−207.

(3) Hu, P. A.; Wang, L. F.; Yoon, M.; Zhang, J.; Feng, W.; Wang, X. N.; Wen, Z. Z.; Idrobo, J. C.; Miyamoto, Y.; Geohegan, D. B.; Xiao, K. Highly Responsive Ultrathin GaS Nanosheet Photodetectors on Rigid and Flexible Substrates. *Nano Lett.* **2013**, *13*, 1649−1654.

(4) Yu, M. M.; Hu, Y. X.; Gao, F.; Dai, M. J.; Wang, L. F.; Hu, P. A.; Feng, W. High-Performance Devices Based on InSe-$In_{1-x}Ga_xSe$ Van der Waals Heterojunctions. *ACS Appl. Mater. Interfaces* **2020**, *12*, 24978−24983.

(5) Dai, M. J.; Chen, H. Y.; Wang, F. K.; Hu, Y. X.; Wei, S.; Zhang, J.; Wang, Z. G.; Zhai, T. Y.; Hu, P. A. Robust Piezo-Phototronic Effect in Multilayer γ-InSe for High-Performance Self-Powered Flexible Photodetectors. *ACS Nano* **2019**, *13*, 7291−7299.

(6) Hu, P. A.; Wen, Z. Z.; Wang, L. F.; Tan, P. H.; Xiao, K. Synthesis of Few-Layer GaSe Nanosheets for High Performance Photodetectors. *ACS Nano* **2012**, *6*, 5988−5994.

(7) Dai, M. J.; Wang, Z. G.; Wang, F. K.; Qiu, Y. F.; Zhang, J.; Xu, C. Y.; Zhai, T. Y.; Cao, W. W.; Fu, Y. Q.; Jia, D. C.; Zhou, Y.; Hu, P. A. Two-Dimensional van der Waals Materials with Aligned In-Plane Polarization and Large Piezoelectric Effect for Self-Powered Piezoelectric Sensors. *Nano Lett.* **2019**, *19*, 5410−5416.

(8) Dai, M. J.; Zheng, W.; Zhang, X.; Wang, S. M.; Lin, J. H.; Li, K.; Hu, Y. X.; Sun, E. W.; Zhang, J.; Qiu, Y. F.; Fu, Y. Q.; Cao, W. W.; Hu, P. A. Enhanced Piezoelectric Effect Derived from Grain Boundary in MoS_2 Monolayers. *Nano Lett.* **2020**, *20*, 201−207.

(9) Thakar, K.; Mukherjee, B.; Grover, S.; Kaushik, N.; Deshmukh, M.; Lodha, S. Multilayer ReS_2 Photodetectors with Gate Tunability for High Responsivity and High-Speed Applications. *ACS Appl. Mater. Interfaces* **2018**, *10*, 36512−36522.

(10) Zhao, K. Y.; Huang, F. M.; Dai, C. M.; Li, W. W.; Chen, S. Y.; Jiang, K.; Huang, Y. P.; Hu, Z. G.; Chu, J. H. Temperature Dependence of Phonon Modes, Optical Constants, and Optical Band Gap in Two-Dimensional ReS_2 Films. *J. Phys. Chem. C* **2018**, *122*, 29464−29469.

(11) Nazir, G.; Rehman, M. A.; Khan, M. F.; Dastgeer, G.; Aftab, S.; Afzal, A. M.; Seo, Y.; Eom, J. Comparison of Electrical and Photoelectrical Properties of ReS_2 Filed-Effect Transistors on Different Dielectric Substrates. *ACS Appl. Mater. Interfaces* **2018**, *10*, 32501−32509.

(12) Xiang, D.; Liu, T.; Wang, J. Y.; Wang, P.; Wang, L.; Zheng, Y.; Wang, Y. N.; Gao, J.; Ang, K. W.; Eda, G.; Hu, W. D.; Liu, L.; Chen, W. Anomalous Broadband Spectrum Photodetection in 2D Rhenium Disulfide Transistor. *Adv. Opt. Mater.* **2019**, *7*, 1901115.

(13) Zhang, E.; Jin, Y. B.; Yuan, X.; Wang, W. Y.; Zhang, C.; Tang, L.; Liu, S. S.; Zhou, P.; Hu, W. D.; Xiu, F. X. ReS_2-Based Field-Effect Transistors and Photodetectors. *Adv. Funct. Mater.* **2015**, *25*, 4076−4082.

(14) An, Q. W.; Liu, Y.; Jiang, R. J.; Meng, X. Q. Chemical Vapor Deposition Growth of ReS_2 Nanowires for High-Performance Nanostructured Photodetector. *Nanoscale* **2018**, *10*, 14976−14983.

(15) Lim, J.; Jeon, D.; Lee, S.; Yu, J. S.; Lee, S. Nucleation Promoted Synthesis of Large-Area ReS_2 Film for High-Speed Photodetectors. *Nanotechnology* **2020**, *31*, 115603.

(16) Xu, J.; Chen, L.; Dai, Y. W.; Cao, Q.; Sun, Q. Q.; Ding, S. J.; Zhu, H.; Zhang, D. W. A Two-Dimensional Semiconductor Transistor with Boosted Gate Control and Sensing Ability. *Sci. Adv.* **2017**, *3*, 1602246.

(17) Kannan, G.; Vasileska, D. The Impact of Surface-Roughness Scattering on the Low-Field Electron Mobility in Nano-Scale Si MOSFETs. *J. Appl. Phys.* **2017**, *122*, 114303.

(18) Liu, E. F.; Fu, Y. J.; Wang, Y. J.; Feng, Y. Q.; Liu, H. M.; Wan, X. G.; Zhou, W.; Wang, B. G.; Shao, L. B.; Ho, C. H.; Huang, Y. S.; Cao, Z. Y.; Wang, L. G.; Li, A. D.; Zeng, J. W.; Song, F. Q.; Wang, X. R.; Shi, Y.; Yuan, H. T.; Hwang, H. Y.; et al. Integrated Digital

Inverters Based on Two-Dimensional Anisotropic ReS_2 Field-Fffect Transistors. *Nat. Commun.* **2015**, *6*, 6991.
(19) Ho, C. H.; Liao, P. C.; Huang, Y. S. Optical Absorption of ReS_2 and $ReSe_2$ Single Crystals. *J. Appl. Phys.* **1997**, *81*, 6380.
(20) Mukherjee, B.; Zulkefli, A.; Hayakawa, R.; Wakayama, Y.; Nakaharai, S. Enhanced Quantum Efficiency in Vertical Mixed-Thickness *n*-ReS_2/*p*-Si Heterojunction Photodiodes. *ACS Photonics* **2019**, *6*, 2277−2286.
(21) Srivastava, P. K.; Hassan, Y.; Gebredingle, Y.; Jung, J.; Kang, B.; Yoo, W. J.; Singh, B.; Lee, C. van der Waals Broken-Gap *p-n* Heterojunction Tunnel Diode Based on Black Phosphorus and Rhenium Disulfide. *ACS Appl. Mater. Interfaces* **2019**, *11*, 8266−8275.
(22) Kang, B.; Kim, Y.; Yoo, W. J.; Lee, C. Ultrahigh Photo-responsive Device Based on ReS_2/Graphene Heterostructure. *Small* **2018**, *14*, 1802593.
(23) Varghese, A.; Saha, D.; Thakar, K.; Jindal, V.; Ghosh, S.; Medhekar, N. V.; Ghosh, S.; Lodha, S. Near-Direct Bandgap WSe_2/ReS_2 Type-II *p-n* Heterojunction for Enhanced Ultrafast Photo-detection and High-Performance Photovoltaics. *Nano Lett.* **2020**, *20*, 1707−1717.
(24) Jariwala, D.; Marks, T. J.; Hersam, M. C. Mixed-Dimensional van der Waals Heterostructures. *Nat. Mater.* **2017**, *16*, 170−181.
(25) Shang, H. M.; Chen, H. Y.; Dai, M. J.; Hu, Y. X.; Gao, F.; Yang, H. H.; Xu, B.; Zhang, S. C.; Tan, B. Y.; Zhang, X.; Hu, P. A. A Mixed-Dimensional 1D Se-2D InSe van der Waals Heterojunction for High Responsivity Self-Powered Photodetectors. *Nanoscale Horiz.* **2020**, *5*, 564−572.
(26) Qin, J. K.; Yan, H.; Qiu, G.; Si, M. W.; Miao, P.; Duan, Y. Q.; Shao, W. Z.; Zhen, L.; Xu, C. Y.; Ye, P. D. Hybrid Dual-Channel Phototransistor Based on 1D t-Se and 2D ReS_2 Mixed-Dimensional Heterostructures. *Nano Res.* **2019**, *12*, 669−674.
(27) Wu, H. L.; Kang, Z.; Zhang, Z. H.; Si, H. N.; Liao, Q. L.; Zhang, S. C.; Wu, J.; Zhang, X. K.; Zhang, Y. Interfacial Charge Behavior Modulation in Perovskite Quantum Dot-Monolayer MoS_2 0D-2D Mixed-Dimensional van der Waals Heterostructures. *Adv. Funct. Mater.* **2018**, *28*, 1802015.
(28) Choi, W.; Akhtar, I.; Kang, D.; Lee, Y. J.; Jung, J.; Kim, Y. H.; Lee, C. H.; Hwang, D. J.; Seo, Y. Optoelectronics of Multijunction Heterostructures of Transition Metal Dichalcogenides. *Nano Lett.* **2020**, *20*, 1934−1943.
(29) Peng, H.; Kioussis, N.; Snyder, G. J. Elemental Tellurium as a Chiral *p*-Type Thermoelectric Material. *Phys. Rev. B: Condens. Matter Mater. Phys.* **2014**, *89*, 195206.
(30) Wang, Q. S.; Safdar, M.; Xu, K.; Mirza, M.; Wang, Z. M.; He, J. van der Waals Epitaxy and Photoresponse of Hexagonal Tellurium Nanoplates on Flexible Mica Sheets. *ACS Nano* **2014**, *8*, 7497−7505.
(31) Lee, T.; Lee, S.; Lee, E.; Sohn, S.; Lee, Y.; Lee, S.; Moon, G.; Kim, D.; Kim, Y. S.; Myoung, J. M.; Wang, Z. L. High-Power Density Piezoelectric Energy Harvesting Using Radially Strained Ultrathin Trigonal Tellurium Nanowire Assembly. *Adv. Mater.* **2013**, *25*, 2920−2925.
(32) Qiu, G.; Huang, S. Y.; Segovia, M.; Venuthurumilli, P. K.; Wang, Y. X.; Wu, W. Z.; Xu, X. F.; Ye, P. D. Thermoelectric Performance of 2D Tellurium with Accumulation Contacts. *Nano Lett.* **2019**, *19*, 1955−1962.
(33) Pham, T.; Oh, S.; Stetz, P.; Onishi, S.; Kisielowski, C.; Cohen, M. L.; Zettl, A. Torsional Instability in the Single-Chain Limit of a Transition Metal Trichalcogenide. *Science* **2018**, *361*, 263−266.
(34) Shen, C. F.; Liu, Y. H.; Wu, J. B.; Xu, C.; Cui, D. Z.; Li, Z.; Liu, Q. Z.; Li, Y. R.; Wang, Y. X.; Cao, X.; Kumazoe, H.; Shimojo, F.; Krishnamoorthy, A.; Kalia, R. K.; Nakano, A.; Vashishta, P. D.; Amer, M. R.; Abbas, A. N.; Wang, H.; Wu, W. Z.; et al. Tellurene Photodetector with High Gain and Wide Bandwidth. *ACS Nano* **2020**, *14*, 303−310.
(35) Amani, M.; Tan, C. L.; Zhang, G.; Zhao, C. S.; Bullock, J.; Song, X. H.; Kim, H.; Shrestha, V. R.; Gao, Y.; Crozier, K. B.; Scott, M.; Javey, A. Solution-Synthesized High-Mobility Tellurium Nanoflakes for Short-Wave Infrared Photodetectors. *ACS Nano* **2018**, *12*, 7253−7263.
(36) Zhang, X.; Jiang, J. Z.; Suleiman, A. A.; Jin, B.; Hu, X. Z.; Zhou, X.; Zhai, T. Y. Hydrogen-Assisted Growth of Ultrathin Te Flakes with Giant Gate-Dependent Photoresponse. *Adv. Funct. Mater.* **2019**, *29*, 1906585.
(37) Thakar, K.; Mukherjee, B.; Grover, S.; Kaushik, N.; Deshmukh, M.; Lodha, S. Multilayer ReS_2 Photodetectors with Gate Tunability for High Responsivity and High-Speed Applications. *ACS Appl. Mater. Interfaces* **2018**, *10*, 36512−36522.
(38) Du, Y. C.; Qiu, G.; Wang, Y. X.; Si, M. W.; Xu, X. F.; Wu, W. Z.; Ye, P. D. One-Dimensional van der Waals Material Tellurium: Raman Spectroscopy under Strain and Magneto-Transport. *Nano Lett.* **2017**, *17*, 3965−3973.
(39) Miao, P.; Qin, J. K.; Shen, Y. F.; Su, H. M.; Dai, J. F.; Song, B.; Du, Y. C.; Sun, M. T.; Zhang, W.; Wang, H. L.; Xu, C. Y.; Xu, P. Unraveling the Raman Enhancement Mechanism on 1T●-Phase ReS_2 Nanosheets. *Small* **2018**, *14*, 1704079.
(40) Zhao, M.; Zhang, W. T.; Liu, M. M.; Zou, C.; Yang, K. Q.; Yang, Y.; Dong, Y. Q.; Zhang, L. J.; Huang, S. M. Interlayer Coupling in Anisotropic/Isotropic van der Waals Heterostructures of ReS_2 and MoS_2 Monolayers. *Nano Res.* **2016**, *9*, 3772−3780.
(41) Brorson, M.; Hansen, T. W.; Jacobsen, C. J. H. Rhenium (IV) Sulfide Nanotubes. *J. Am. Chem. Soc.* **2002**, *124*, 11582−11583.
(42) Wang, H.; Tong, Z. Q.; Yang, R.; Huang, Z. M.; Shen, D.; Jiao, T. P.; Cui, X.; Zhang, W. J.; Jiang, Y.; Lee, C. S. Electrochemically Stable Sodium Metal-Tellurium/Carbon Nanorods Batteries. *Adv. Energy Mater.* **2019**, *9*, 1903046.
(43) Liu, E.; Long, M. S.; Zeng, J. W.; Luo, W.; Wang, Y. J.; Pan, Y. M.; Zou, W.; Wang, B. G.; Hu, W. D.; Ni, Z. H.; You, Y. M.; Zhang, X. A.; Qin, S. Q.; Shi, Y.; Watanabe, K.; Taniguchi, T.; Yuan, H. T.; Hwang, H. Y.; Cui, Y.; Miao, F.; Ding, X. High Responsivity Phototransistors Based on Few-Layer ReS_2 for Weak Signal Detection. *Adv. Funct. Mater.* **2016**, *26*, 1938−1944.
(44) Zhuo, R.; Zeng, L.; Yuan, H.; Wu, D.; Wang, Y.; Shi, Z.; Xu, T.; Tian, Y.; Li, X.; Tsang, Y. H. *In-Situ* Fabrication of $PtSe_2$/GaN Heterojunction for Self-Powered Deep Ultraviolet Photodetector with Ultrahigh Current on/off Ratio and Detectivity. *Nano Res.* **2019**, *12*, 183−189.
(45) Qin, J. K.; Qiu, G.; He, W.; Jian, J.; Si, M. W.; Duan, Y. Q.; Charnas, A.; Zemlyanov, D. Y.; Wang, H. Y.; Shao, W. Z.; Zhen, L.; Xu, C. Y.; Ye, P. D. Epitaxial Growth of 1D Atomic Chain Based Se Nanoplates on Monolayer ReS_2 for High-Performance Photo-detectors. *Adv. Funct. Mater.* **2018**, *28*, 1806254.
(46) Kufer, D.; Nikitskiy, I.; Lasanta, T.; Navickaite, G.; Koppens, F. H. L.; Konstantatos, G. Hybrid 2D-0D MoS_2-PbS Quantum Dot Photodetectors. *Adv. Mater.* **2015**, *27*, 176−180.
(47) Sun, J. C.; Wang, Y. Y.; Guo, S. Q.; Wan, B. S.; Dong, L. Q.; Gu, Y. D.; Song, C.; Pan, C. F.; Zhang, Q. H.; Gu, L.; Pan, F.; Zhang, J. Y. Lateral 2D WSe_2 *p-n* Homojunction Formed by Efficient Charge-Carrier-Type Modulation for High-Performance Optoelectronics. *Adv. Mater.* **2020**, *32*, 1906499.
(48) Mukherjee, B.; Zulkefli, A.; Hayakawa, R.; Wakayama, Y.; Nakaharai, S. Enhanced Quantum Efficiency in Vertical Mixed-Thickness *n*-ReS_2/*p*-Si Heterojunction Photodiodes. *ACS Photonics* **2019**, *6*, 2277−2286.
(49) Zhou, N.; Wang, R. Y.; Zhou, X.; Song, H. Y.; Xiong, X.; Ding, Y.; Lü, J. T.; Gan, L.; Zhai, T. Y. *p*-GaSe/*n*-MoS_2 Vertical Heterostructures Synthesized by van der Waals Epitaxy for Photo-response Modulation. *Small* **2018**, *14*, 1702731.
(50) Sun, G. Z.; Li, B.; Li, J.; Zhang, Z. W.; Ma, H. F.; Chen, P.; Zhao, B.; Wu, R. X.; Dang, W. Q.; Yang, X. D.; Tang, X. W.; Dai, C.; Huang, Z. W.; Liu, Y.; Duan, X. D.; Duan, X. F. Direct van der Waals Epitaxial Growth of 1D/2D Sb_2Se_3/WS_2 Mixed Dimensional *p-n* Heterojunctions. *Nano Res.* **2019**, *12*, 1139−1145.
(51) Ra, H. S.; Kwak, D. H.; Lee, J. S. A Hybrid MoS_2 Nanosheet-CdSe Nanocrystal Phototransistor with a Fast Photoresponse. *Nanoscale* **2016**, *8*, 17223−17230.
(52) Cao, R.; Zhang, Y.; Wang, H. D.; Zeng, Y. H.; Zhao, J. L.; Zhang, L. Y.; Li, J. Q.; Meng, F. X.; Shi, Z.; Fan, D. Y.; Guo, Z. N. Solar-Blind Deep-Ultraviolet Photodetectors Based on Solution-

https://dx.doi.org/10.1021/acsnano.0c09912
ACS Nano 2021, 15, 3241−3250

Synthesized Quasi-2D Te Nanosheets. *Nanophotonics* **2020**, *9*, 2459−2466.
(53) Zhang, Y.; Xu, W. X.; Xu, X. J.; Yang, W.; Li, S. Y.; Chen, J. X.; Fang, X. S. Low-Cost Writing Method for Self-Powered Paper-Based UV Photodetectors Utilizing Te/TiO_2 and Te/ZnO Heterojunctions. *Nanoscale Horiz.* **2019**, *4*, 452−456.
(54) Zheng, W.; Feng, W.; Zhang, X.; Chen, X. S.; Chen Liu, G. B.; Qiu, Y. F.; Hasan, T.; Tan, P. H.; Hu, P. A. Anisotropic Growth of Nonlayered CdS on MoS_2 Monolayer for Functional Vertical Heterostructures. *Adv. Funct. Mater.* **2016**, *26*, 2648−2654.
(55) Ghamgosar, P.; Rigoni, F.; Kohan, M. G.; You, S. J.; Morales, E. A.; Mazzaro, R.; Morandi, V.; Almqvist, N.; Concina, I.; Alberto Vomiero, A. Self-Powered Photodetectors Based on Core-Shell ZnO-Co_3O_4 Nanowire Heterojunctions. *ACS Appl. Mater. Interfaces* **2019**, *11*, 23454−23462.
(56) Qin, J. K.; Shao, W. Z.; Xu, C. Y.; Li, Y.; Ren, D. D.; Song, X. G.; Zhen, L. Chemical Vapor Deposition Growth of Degenerate *p*-Type Mo-Doped ReS_2 Films and Their Homojunction. *ACS Appl. Mater. Interfaces* **2017**, *9*, 15583−15591.
(57) Treusce, J.; Sandrock, R. Energy Band Structure of Selenium and Tellurium. *Phys. Status Solidi B* **1966**, *16*, 487−497.
(58) Bai, F.; Qi, J.; Li, F.; Fang, Y.; Han, W.; Wu, H.; Zhang, Y. A High-Performance Self-Powered Photodetector Based on Monolayer MoS_2/Perovskite Heterostructures. *Adv. Mater. Interfaces* **2018**, *5*, 1701275.
(59) Ma, C.; Shi, Y. M.; Hu, W. J.; Chiu, M. H.; Liu, Z. X.; Bera, A.; Li, F.; Wang, H.; Li, L. J.; Wu, T. Heterostructured WS_2/$CH_3NH_3PbI_3$ Photoconductors with Suppressed Dark Current and Enhanced Photodetectivity. *Adv. Mater.* **2016**, *28*, 3683−3689.
(60) Zhou, X.; Zhou, N.; Li, C.; Song, H. Y.; Zhang, Q.; Hu, X. Z.; Gan, L.; Li, H. Q.; Lü, J. T.; Luo, J.; Xiong, J.; Zhai, T. Y. Vertical Heterostructures Based on $SnSe_2$/MoS_2 for High Performance Photodetectors. *2D Mater.* **2017**, *4*, 025048.
(61) Ra, H. S.; Kwak, D. H.; Lee, J. S. A Hybrid MoS_2 Nanosheet-CdSe Nanocrystal Phototransistor with a Fast Photoresponse. *Nanoscale* **2016**, *8*, 17223−17230.
(62) Wang, Y.; Tang, Z. Y.; Podsiadlo, P.; Elkasabi, Y.; Lahann, J.; Kotov, N. A. Mirror-Like Photoconductive Layer-by-Layer Thin Films of Te Nanowires: The Fusion of Semiconductor, Metal, and Insulator Properties. *Adv. Mater.* **2006**, *18*, 518−522.

https://dx.doi.org/10.1021/acsnano.0c09912
ACS Nano 2021, 15, 3241−3250